Automatic identification of intraretinal cystoid regions in Optical Coherence Tomography

Joaquim de Moura[1], Jorge Novo[1], José Rouco[1], M.G. Penedo[1], and Marcos Ortega[1]
{joaquim.demoura, jnovo, jrouco, mgpenedo, mortega}@udc.es

University of A Coruña. Department of Computer Science, A Coruña (Spain)

Abstract. Optical Coherence Tomography (OCT) is, nowadays, one of the most referred ophthalmological imaging techniques. OCT imaging offers a window to the eye fundus in a non-invasive way, permitting the inspection of the retinal layers in a cross sectional visualization. For that reason, OCT images are frequently used in the analysis of relevant diseases such as hypertension or diabetes. Among other pathological structures, a correct identification of cystoid regions is a crucial task to achieve an adequate clinical analysis and characterization, as in the case of the analysis of the exudative macular disease.
This paper proposes a new methodology for the automatic identification of intraretinal cystoid fluid regions in OCT images. Firstly, the method identifies the Inner Limitant Membrane (ILM) and Retinal Pigment Epithelium (RPE) layers that delimit the region of interest where the intraretinal cystoid regions are placed. Inside these limits, the method analyzes windows of a given size and determine the hypothetical presence of cysts. For that purpose, a large and heterogeneous set of features were defined to characterize the analyzed regions including intensity and texture-based features. These features serve as input for representative classifiers that were included in the analysis.
The proposed methodology was tested using a set of 50 OCT images. 502 and 539 samples of regions with and without the presence of cysts were selected from the images, respectively. The best results were provided by the LDC classifier that, using a window size of 61×61 and 40 features, achieved satisfactory results with an accuracy of 0.9461.

Keywords: Computer-aided diagnosis, retinal imaging, Optical Coherence Tomography, intraretinal cystoid regions

1 Introduction and previous work

The analysis of the retina is crucial for the diagnosis of different relevant pathologies. For that reason, the identification of the main retinal structures as the optic disc [1] or the vascular tree [2] can provide evidences for an appropriate characterization of diseases like hypertension or diabetes. Among the different image modalities, Optical Coherence Tomography (OCT) have spread their use over

the years as they offer a cross-sectional view of the retina and sub-retinal layers with microscopic resolution in a non-invasive and contactless way, providing a more detailed source of information than other modalities such as retinographies. This more detailed set of information about the retinal layers can help the specialists to perform more accurate analysis of relevant diseases as age-related macular degeneration (AMD) or glaucoma [3].

AMD can lead to exudative macular disease, one of the main causes of blindness in developed countries. The intraretinal cystoid fluid is directly related with exudative macular disease, originated by abnormal vasculature growing that leaks fluid, deriving in a progressive retinal architecture degeneration and the corresponding vision loss (Fig. 1). For that reason, an appropriate identification and characterization of the cystoid regions is a crucial task as it represents a measurement of the disease severity, helping clinicians to produce more accurate diagnosis and treatments [4].

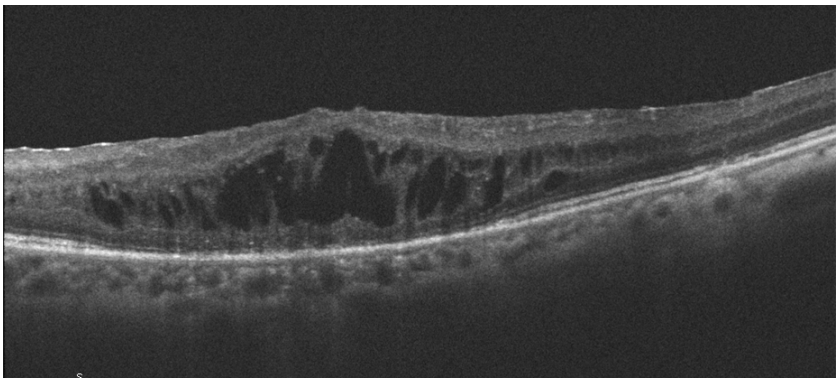

Fig. 1. Example of OCT image with the presence of intraretinal cystoid regions.

In recent years, some works have been proposed facing the issue of cyst extraction. The proposals frequently used an initial denoising stage to minimize the impact of the typical speckle noise that normally appears in OCT imaging. Most of the approaches addressed directly the problem by the segmentation of cyst candidates followed by a morphological and intensity analysis and/or a post-processing stage to reduce the false positive (FP) detections and return the final results. Following this strategy, Wilkins *et al.* [5] faced the cystoid macular edema identification by an initial thresholding of dark structures to identify the cyst candidate contours. They posteriorly applied a couple of rules to reduce the FP detections and produce the final identifications. Roychowdhury *et al.* [6] also segments dark regions in a bright neighborhood after identifying the 6 main retinal layers. This cyst candidate set is posteriorly analyzed in terms of solidity, mean and maximum intensities to produce the final cyst identifications. In the case of Wieclawek *et al.* [7], a combination of image processing techniques were applied to extract the candidate segmentations. Redundant regions are posteriorly removed to produce the final cyst extractions. González *et al.* [8] used watershed to produce the initial candidates segmentation. The extracted re-

gions are posteriorly grouped by connectivity and similarity in terms of intensity. Given the large amount of FPs that this step produces, the method posteriorly filters the candidates using discarding rules combined with a learning strategy to reduce the FPs set. Esmaeili *et al.* [9] used a K-SVD dictionary learning in curvelet transform to help with the speckle noise reduction and facilitate the posterior thresholding strategy that the authors proposed. Miss-extractions are posteriorly removed in a post-processing stage. A combined strategy for cysts segmentation was proposed by Wang *et al.* [10], using a fuzzy level set that integrates fuzzy C-Means and level sets. The method extracts the fluid regions by intensity, thanks to the fuzzy C-Means, with a adequate contour segmentation, incorporated by the level set method. The work of Xu *et al.* [11] defined a layer-dependent stratified sampling to produce symptomatic exudate-associated derangements segmentations using voxel classification. In the case of Lang *et al.* [12] a pixel classification system was also designed, but limited to the domain of micro-cystic segmentations.

This strategy, that was followed by most of the approaches, presents as main limitation the high dependency in the candidate segmentation stage. A poor segmentation technique may produce initial large candidate sets, hardening the posterior refinement to remove the detected FPs. Large sets of FPs can provoke the necessity of strong reduction stages that may carry the elimination of real cysts. Additionally, incorrect cyst candidate segmentations may also alter the candidate characteristics, deriving in confusions in the posterior morphological/intensity analysis, penalizing the final cyst identification results.

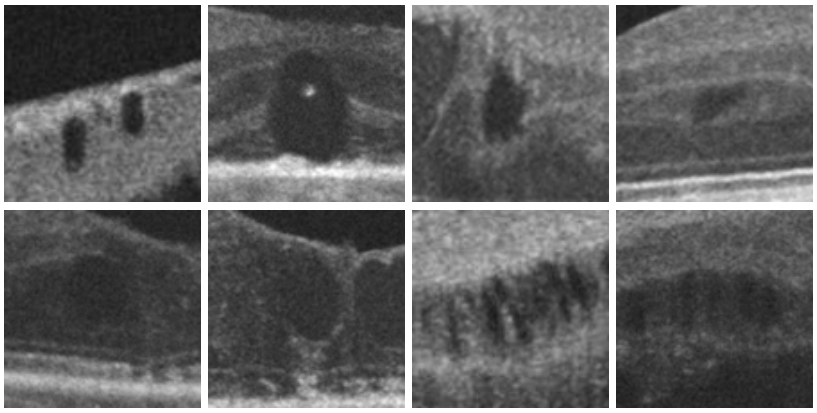

(a) (b) (c) (d)

Fig. 2. Examples of cysts with different levels of complexity.

Many times, this segmentation dependency can be overcome as fluid regions and cyst contours can be acceptably obtained, as illustrated with the examples of Fig. 2, 1^{st} row. However, many other times, the cyst contours cannot be clearly identified as there is no enough intensity contrast in the entire cyst region (Fig. 2, second row, (a) & (b)). Other times, cysts appear in nearby groups, making

extremely complicated the identification and delimitation of all of them, even for the human eye of the experts (Fig. 2, second row, (c) & (d)).

In this work, we propose a new methodology that faces the issue of cyst identification with a novel strategy. Instead of classical cyst candidate segmentations and FPs removal, we identify intraretinal cystoid regions, that is, regions of the OCT images that contain cysts. The method uses a window size for the analysis, extracts a set of image characteristics and determines the presence of cysts inside the analyzed regions.

2 Methodology

The proposed system firstly identify the retinal layer limits that contain the intraretinal cystoid regions. Then, inside this region of interest, the method analyze windows of a defined size to identify the cyst presence including: feature measurement, feature selection and classification.

2.1 Retinal layer segmentation

As cysts appear inside the retinal layers, we can reduce the search space identifying this region of the OCT images. The region of interest is delimited between the Inner Limitant Membrane (ILM), first intraretinal layer, and the Retinal Pigment Epithelium (RPE), formed by pigmented cells at the external part of the retina.

For that purpose, we used a method based on the work of Chiu *et al.* [13]. This method uses graph theory to represent each image as a graph of nodes. Then, the optimum connected paths from both sides of the image are obtained using dynamic programming. In this case, dark-to-light gradient images are firstly calculated as these gradients identify the limits of adjacent layers. These gradients are used to generate weights for the layer segmentations. The minimum weighted paths are found by the Dijkstra's algorithm [14] to progressively identify the main layers of the retina. Despite this approach was designed to find eight different layers, we aimed in this work for the ILM and RPE layers, as they constitute the limits of the retinal layers, sufficient for the delimitation of the intraretinal cysts search space. Fig. 3 shows an example of ILM and RPE layer identification for a particular OCT image.

2.2 Feature measurement

In order to characterize each analyzed region and identify the presence of cysts, a complete set of 189 features was defined. This feature set includes intensity and texture-based properties that help to maximize the discrimination power of cysts identification with respect to other structures and patterns of the retina.

Intensity statistics We measured 13 global characteristics of the analyzed region, including: *maximum, minimum, mean, median, standard deviation, variance,* 25^{th} *and* 75^{th} *percentile, skewness* and *maximum likelihood estimates for a normal distribution.*

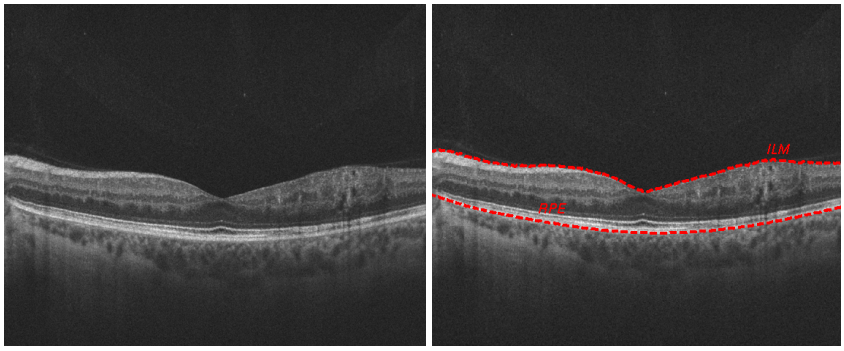

Fig. 3. Example of ILM and RPE retinal layer segmentation.

Gray-level Intensity Histogram (GLIH) Using the intensity histogram of the analyzed region, the method derives the following measurements: *obliquity, kurtosis, energy* and *entropy*.

Eigenvalues Eigenvalues can be useful to capture regions with intensity changes in different directions, as happens with the presence of cysts. We calculated the eigenvalues of the analyzed region and selected the 4 highest (λ_{max_i}) and the 2 lowest (λ_{min_i}) values. Additionally, several ratios among them were also included in the feature set.

Histogram of Oriented Gradients (HOG) The orientation of the gradients can be useful in this issue as cysts typically present closed/oval contours. Instead of that, non-cystoid regions present a more uniform shape, with lower levels of gradients and, if present, they usually appear with a parallel horizontal pattern (due to the presence of the retinal layers) or vertical and tubular patterns (due to the shadows of vessels or other structures). HOG features [15] can help to capture these patterns, presenting some invariance to scale, rotation or translation changes, properties also useful in this issue. 9 HOG windows per bound box and 9 histogram bins were analyzed, adding a total of 81 characteristics.

Local binary patterns (LBP) LBPs [16] can help to identify local patterns that may appear with and without the presence of cysts. LBPs presents a low complexity and a low sensitivity to changes in illumination, common conditions in OCT imaging due to the variability of capture machines and configuration parameters. A wide range was analyzed, calculating a total of 64 features that were added to the feature set.

Gray-Level Co-Ocurrence Matrix (GLCM) These second order statistics measure the simultaneous ocurrence of gray levels in pairs of pixels, separated by a displacement vector. Based on the proposal of Haralick *et al.* [17], we performed the analysis at a distance of 2 pixels and 4 directions: 0°, 45°, 90° and 135°, obtaining a total of 16 features.

2.3 Feature selection and classification

Next step involves feature selection to avoid irrelevant and redundant characteristics by selecting the most useful ones and, therefore, facilitating the classification stage. Sequential forward selection using, as criterion, inter-intra feature distance was used.

Finally, representative classifiers, frequently used in medical imaging solutions, were trained and tested using the extracted feature set: Linear Discriminant Analysis (LDA), $k-$nearest neighbors (kNN) and Support Vector Machines (SVM) were analyzed. In the case of kNN, 3 configurations were tested using $k = [3, 5, 7]$ whereas 3 configurations were also defined for the case of the SVM, using an exponential kernel with values of $\theta = [1, 2, 3]$:

$$k(x, y) = exp\left(-\frac{\parallel x - y \parallel}{\theta}\right) \tag{1}$$

The classification stage was done using a constructed dataset that was randomly divided in two smaller datasets with the same size (each one with the 50% of all the samples). The first dataset is used for the training stage whereas the second one is reserved for testing the trained classifiers. This process of dataset random division, training and testing was repeated 50 times, calculating the mean accuracy in order to obtain a global performance measurement.

3 Results and discussion

The proposed method was validated using a set of 50 OCT histological images. These images were captured by a confocal scanning laser ophtalmoscope, a CIRRUS^{TM}HD-OCT–Carl Zeiss Meditec. The images correspond to scans centered in the macula, from both left and right eyes of different patients, and with resolutions that vary from 924×616 to 1200×800. Several intensity and contrast configurations are also present in the image set. No preprocessing was applied to the images.

The images were labeled by an expert clinician, identifying the location of any present cyst. Using this information, we constructed a dataset by the selection of 502 and 539 samples of regions with and without the presence of cysts, using a window size of 61×61. As said, this dataset was randomly divided in two smaller datasets with the same size, one for training and other for testing, using 50 repetitions for each configuration to obtain, for each case, a global measurement of its performance.

Regarding the selected features, the majority of them were taken from HOG and also from LBP feature sets as they include a high potential in the differentiation of common layer patterns and other structures with respect to the cyst presence. Global intensity statistics, as *minimum*, were also selected in the first positions as the cyst presence typically implies a depression in intensity values and changes in intensity profiles of the analyzed window.

Table 1 presents the accuracy results that were achieved by the different classifier configurations using progressive larger feature sets. A maximum of 50

Table 1. Accuracy results that were obtained with the tested classifiers using different feature set sizes.

N. Features	**1**	**5**	**10**	**30**	**50**
LDC	0.7747	0.8721	0.9016	0.9394	0.9456
3-kNN	0.7140	0.8568	0.8870	0.9088	0.9110
5-kNN	0.7348	0.8626	0.8986	0.9099	0.9142
7-kNN	0.7453	0.8617	0.8920	0.9067	0.9049
1-SVM	0.7692	0.8698	0.9043	0.9270	0.9262
2-SVM	0.7742	0.8652	0.9014	0.9196	0.9219
3-SVM	0.7747	0.8638	0.8986	0.9157	0.9165

features was set as no further improvements were obtained from that point, achieving the best performance of each case with smaller feature sets, as Table 2 details. Generally, the obtained accuracy results in all the cases are significantly high, being the best results obtained with the LDC classifier and 40 features, returning a performance of 0.9461. In the case of the SVM, it offers better results than the kNN, being the lowest value the case of the 7-kNN, with a performance of 0.9099. The results of the first degree SVM are significantly high, 0.9299, but at a distance of the LDC classifier.

Table 2. Best accuracy obtained by each tested classifier, indicating the number of needed features.

Classifier	*LDC*	*3-kNN*	*5-kNN*	*7-kNN*	*1-SVM*	*2-SVM*	*3-SVM*
N. Features	40	42	44	43	44	44	28
Accuracy	0.9461	0.9136	0.9151	0.9099	0.9299	0.9240	0.9202

Fig. 4 shows some examples of cystoid and non-cystoid regions from the testing dataset that were correctly classified. Regarding non-cystoid regions, the method is capable to identify the tissue and layer patterns with different levels of intensity and contrast (Fig. 4(a) & (b)) but also to discard dark patterns that are derived from shadows of vessels and other artifacts (Fig. 4(a),(c) & (d)). In the case of the cystoid regions, we can see that the method is capable to detect the simple cases (Fig. 4(a)) where cyst regions and contours are clearly delimited but also other complex cases of cysts or groups with low contrast and imperfect contour definition (Fig. 4(b),(c) & (d)).

Fig. 5 includes some representative incorrect classifications. Many misclassified cystoid regions are omitted due to extremely poor contrast and too fuzzy contours (Fig. 5(a) & (b)) being extremely complicated to detect its presence by the system. The common mistakes in non-cystoid regions are due to the presence of other structures (Fig. 5(c) & (d)) that create artificial high-to-low intensity regions that may be confused with the typical patterns that appear with cysts.

We also tested the performance of the system using progressive window sizes. In the dataset construction, we built the corresponding datasets using the same central points in all the cases but using progressive lower window sizes. Table 3 details the best performances that were achieved with each window size and the best configurations of the SVM, KNN and LDC classifiers. As we can see,

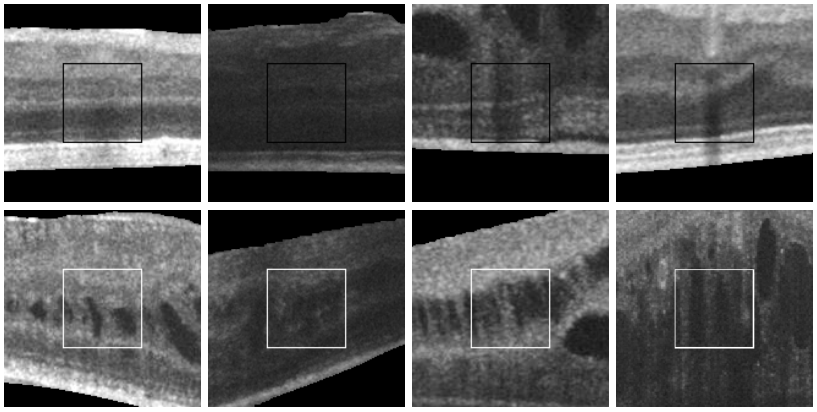

(a) (b) (c) (d)

Fig. 4. Examples of testing samples correctly classified. 1^{st} row, non-cystoid regions. 2^{nd} row, cystoid regions.

the performance is progressively penalized with smaller windows, as they do not offer the same information to identify the presence of cysts in the samples, specially in the cases of windows that include large cysts. The final window size should be selected as a balance between detail in the detections and accuracy in the performance.

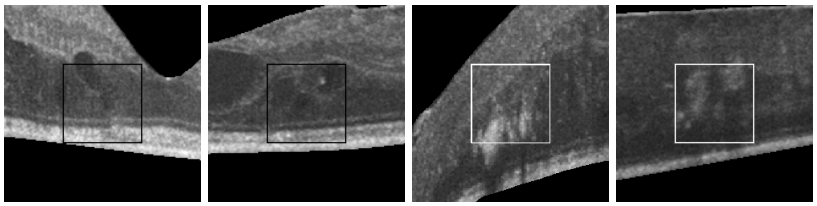

(a) (b) (c) (d)

Fig. 5. Examples of testing samples incorrectly classified. (a) & (b), cystoid regions classified as non-cystoid. (c) & (d), non-cystoid regions classified as cystoid.

Table 3. Best accuracy obtained by each tested classifier using different window sizes.

Window size	*11×11*	*15×15*	*21×21*	*31×31*	*61×61*
LDC	0.8599	0.8906	0.9118	0.9339	0.9461
5-kNN	0.8450	0.8581	0.8872	0.9081	0.9151
1-SVM	0.8654	0.8915	0.9103	0.9247	0.9299

4 Conclusions

The extraction and analysis of intraretinal cystoid fluid regions is a relevant issue for the diagnosis and treatment of relevant pathologies as can represent the exudative macular disease, one of the main causes of blindness in developed countries. Most of the existing approaches faced this issue by an initial segmentation of cyst candidates, segmentations that are posteriorly analyzed using intensity or morphological properties to discard wrong detections. These strategies present a high dependency in the performance of the candidates segmentation stage, given the complex conditions that are frequently present in OCT images. Imperfect or wrong segmentations may carry, in many cases, the removal of existing cysts or the preservation of FPs by the posterior analysis and refinement, penalizing the performance of any proposed system.

In this work, we propose a novel methodology for the identification of intraretinal cystoid fluid regions in OCT images. We face the issue with a different strategy, by the analysis of regions inside the retinal layers and the determination of the presence of cysts. Hence, the dependency of the segmentation stage is omitted, detecting directly the cystoid regions inside the OCT images.

The system defined a set of 189 features, being selected the ones with higher power of discrimination. A set of representative classifiers were studied, including 3 SVM and 3 kNN configurations as well as the LDC classifier. The method was validated with a set of 1041 samples, including 502 and 539 samples of cystoid and non-cystoid regions, respectively. Satisfactory results were obtained, being the best performance achieved by the LDC classifier that, using 40 features and a window size of 61×61, reported an accuracy of 0.9461.

As future work, a further analysis and inclusion of suitable characteristics should be done as well as the use of wrapped based feature selection methods. Moreover, a wider range of classifiers, like artificial neural networks, should be tested in the classification stage.

Acknowledgments This work is supported by the Instituto de Salud Carlos III, Government of Spain and FEDER funds of the European Union through the PI14/02161 and the DTS15/00153 research projects and by the Ministerio de Economía y Competitividad, Government of Spain through the DPI2015-69948-R research project.

References

1. J. Novo, M.G. Penedo, and J. Santos. Optic disc segmentation by means of GA-Optimized Topological Active Nets. *Lecture Notes in Computer Science: Image Analysis and Recognition, ICIAR'08*, 5112:807–816, 2008.
2. J. de Moura, J. Novo, M. Ortega, and P. Charlón. 3D retinal vessel tree segmentation and reconstruction with OCT images. *Lecture Notes in Computer Science: Image Analysis and Recognition, ICIAR'16*, 9730:807–816, 2016.

3. W. Geitzenauer, C.K. Hitzenberger, and U.M. Schmidt-Erfurth. Retinal optical coherence tomography: past, present and future perspectives. *British Journal of Ophthalmology*, 95(2):171–177, 2011.
4. H. Bogunovic, M.D. Abramoff, L. Zhang, and M. Sonka. Prediction of treatment response from retinal oct in patients with exudative age-related macular degeneration. *Ophth. Med. Image Analysis Workshop, MICCAI'14*, pages 129–136, 2014.
5. G.R. Wilkins, O.M. Houghton, and A.L. Oldenburg. Automated segmentation of intraretinal cystoid fluid in optical coherence tomography. *IEEE Transactions on Biomedical Engineering*, 59(4):1109–1114, 2012.
6. S. Roychowdhury, D.D. Koozekanani, S. Radwan, and K.K. Parhi. Automated localization of cysts in diabetic macular edema using optical coherence tomography images. *International Conference of the IEEE Engineering in Medicine and Biology Society*, pages 1426–1429, 2013.
7. W. Wieclawek. Automatic cysts detection in optical coherence tomography images. *Int. Conf. Mixed Design of Integrated Circuits and Systems*, pages 79–82, 2015.
8. A. González, B. Remeseiro, M. Ortega, M.G. Penedo, and P. Charlón. Automatic cyst detection in OCT retinal images combining region flooding and texture analysis. *IEEE Int. Symp. on Computer-Based Medical Systems*, pages 397–400, 2013.
9. M. Esmaeili, A.M. Dehnavi, H. Rabbani, and F. Hajizadeh. Three-dimensional segmentation of retinal cysts from spectral-domain optical coherence tomography images by the use of three-dimensional curvelet based K-SVD. *Journal of Medical Signals and Sensors*, 6(3):166–171, 2016.
10. J. Wang, M. Zhang, A.D. Pechauer, L. Liu, T.S. Hwang, D. Wilson, D.J. Li, and Y. Jia. Automated volumetric segmentation of retinal fluid on optical coherence tomography. *Biomedical Optic Express*, 7(4):1577–1589, 2016.
11. X. Xu, K. Lee, L. Zhang, M. Sonka, and M.D. Abràmoff. Stratified sampling voxel classification for segmentation of intraretinal and subretinal fluid in longitudinal clinical OCT data. *IEEE Transactions on Medical Imaging*, 34(7):1616–1623, 2015.
12. A. Lang, A. Carass, E.K. Swingle, O. Al-Louzi, P. Bhargava, S. Saidha, H.S. Ying, P.A. Calabresi, and J.L. Prince. Automatic segmentation of microcystic macular edema in OCT. *Biomedical Optic Express*, 6(1):155–169, 2014.
13. S.J. Chiu, X.T. Li, P. Nicholas, C.A. Toth, J.A. Izatt, and S. Farsiu. Automatic segmentation of seven retinal layers in SDOCT images congruent with expert manual segmentation. *Optics Express*, 10(10):19413–19428, 2010.
14. E.W. Dijkstra. A note on two problems in connexion with graphs. *Numerische Mathematik*, 1(1):269–271, 1959.
15. N. Dalal and B. Triggs. Histograms of oriented gradients for human detection. *Computer Vision and Pattern Recognition, CVPR'05*, pages 886–893, 2005.
16. T. Ojala, M. Pietikainen, and T. Maenpaa. Multiresolution gray-scale and rotation invariant texture classification with local binary patterns. *IEEE Transactions on Pattern Analysis and Machine Intelligence*, 24(7):971–971, 2002.
17. R.M. Haralick, K. Shanmugam, and I.H. Dinstein. Textural features for image classification. *Systems, Man and Cybernetics, IEEE Trans. on*, (6):610–621, 1973.